ELSEVIER

International Journal of Heat and Fluid Flow 19 (1998) 259–269

International Journal of HEAT AND FLUID FLOW

An experimental study of in-tube evaporation of R-22 inside a 6.5-mm smooth tube

Chi-Chuan Wang [a,*], Ching-Shan Chiang [b], Jyh-Goang Yu [b]

[a] *Energy & Resources Laboratories, Industrial Technology Research Institute, D500 ERL/ITRI, Building 64, 195-6 Section 4, Chung Hsing Road, Chutung, Hsinchu 310, Taiwan, ROC*

[b] *Department of Mechanical Engineering, National Chiao Tung University, Hsinchu 300, Taiwan, ROC*

Received 7 January 1997; received in revised form 9 December 1997; accepted 19 December 1997

Abstract

Two-phase flow pattern, friction, and heat transfer characteristics for R-22 inside a 6.5 mm smooth tube are reported in this study. The range of mass flux is between 50 and 700 kg/m^2 s. The flow pattern map proposed by Weisman et al. (Weisman, J., Duncan, D., Gibson, J., Crawford, T., 1979. Effect of fluid properties and pipe diameter on two-phase flow pattern in horizontal lines. Int. J. Multiphase Flow 5, 437–462) gave a satisfactory flow pattern prediction, and the Klimenko and Fyodorov (Klimenko, V.V., Fyodorov, M., 1990. Prediction of heat transfer for two-phase forced flow in channels of different orientation. In: Proceedings of the Ninth International Heat Transfer Conference, vol. 6, pp. 65–70) criterion shows an excellent classification of the stratified and unstratified flow pattern. The two-phase multipliers are strongly related to the flow pattern, and it is found that the two-phase multiplier is dependent upon mass velocities for stratified-wavy flow pattern. In addition, the two-phase heat transfer coefficient for stratified-wavy flow pattern is found to be insensitive to the change of vapor quality, and is approximately proportional to $q^{0.6-0.7}$.

Keywords: Flow pattern; Two-phase flow; R-22; Heat transfer; Pressure drops

Notation

A_o	outside heat transfer area of the tube, m^2
A_i	nominal inside heat transfer area of the tube, m^2
C	constant in Chisholm correlation
Cp	specific heat of water, J/kg K
dP_f	measured two-phase frictional pressure difference, N/m^2
$dP_{f,l}$	frictional pressure difference for liquid flowing alone, N/m^2
$dP_{f,v}$	frictional pressure difference for gas flowing alone, N/m^2
ΔP_a	pressure drop due to acceleration, N/m^2
ΔP_f	frictional pressure drop, N/m^2
D_i	inside diameter of the tube, m
F	constant in Klimenko and Fyodorov criterion
f_l	friction factor for subcooled liquid
Fr	Froude number
G	mass flux, kg/m^2 s
g	gravitation constant, N/m
h_i	inside heat transfer coefficient, W/m^2 K
h_o	heat transfer coefficient on the annulus side, W/m^2 K
L	effective heating length, m
LMTD	log mean temperature difference, K
$\dot{m}_r$	average mass flow rate of refrigerant, kg/s
$\dot{m}_{water}$	average mass flow rate of coolant water, kg/s
P_r	reduced pressure
q	average heat flux, W/m^2
Q	average heat transfer rate, W
R_p	surface roughness, μm
R_w	wall resistance, W/m^2 K
$T_{water,in}$	inlet temperature of water at annulus side, K
$T_{water,out}$	outlet temperature of water at annulus side, K
T_{sat}	saturation temperature of the refrigerant, K
ΔT	temperature rise on the water coolant, K
ΔT_1	temperature difference, $\Delta T_1 = T_s - T_1$, K
ΔT_2	temperature difference, $\Delta T_2 = T_s - T_2$, K
U_o	overall heat transfer coefficient, W/m^2 K
x	vapor quality
X	Martinelli parameter
Δx	difference of quality

Greek

ρ	density of refrigerant, kg/m^3
λ	latent heat of evaporating vapor, J/kg
ϕ_v^2	two phase friction multiplier for vapor flowing alone
μ	dynamic viscosity of refrigerant, N s/m^2
v	kinematic viscosity of refrigerant, m^2/s
σ	surface tension of refrigerant, N/m

* Corresponding author. E-mail: f781058@erlb.erl.itri.org.tw.

0142-727X/98/$19.00
PII: S0142-727X(98)00006-X

Subscript

L	liquid phase
G	gas phase
ave	average value
1	inlet
2	outlet
i	inside
in	inlet
mod	modified value
o	outside
out	outlet
w	wall
water	water

1. Introduction

In-tube evaporation heat transfer is very important for a wide range of applications such as refrigeration and air-conditioning systems, chemical process, nuclear and conventional power plants. A better understanding of the heat transfer/friction mechanism may be valuable in the design of efficient heat exchangers. Over the past decade, there have been major advancements in the manufacturing technology of efficient heat exchangers. Consequently, this has allowed the use of smaller and higher performance heat exchangers. For example, the use of smaller diameter tubes is becoming popular in the design of HVAC&R (Heating, ventilating, air-conditioning, and refrigeration) fin-and-tube heat exchangers. Smaller tubes can not only significantly improve the air side performance, but also reduce the refrigerant charge as well. Eventually, a considerable size-reduction of heat exchanger can be achieved.

For HVAC&R applications, numerous investigators have conducted experiments on in-tube evaporation and condensation heat transfer characteristics. However, the majority of the studies focused upon heat transfer alone. The friction characteristics were usually not presented. Both heat transfer and friction characteristics are important in the two-phase flow. To correctly predict the thermal-fluids behaviors, it is helpful to identify the two-phase flow pattern within the tube. Unfortunately, most previous two-phase flow pattern studies were associated with diameters on the order of 9.5–75 mm and tested at mass velocities greater than 300 kg/m^2 s as described by Wambsganss et al. (1991). Generally, this corresponds to the annular flow pattern. However, in HVAC&R application, tubes having a diameter less than 9.5 mm with mass velocities less than 300 kg/m^2 s are often encountered. Very few systematic studies addressed this region. Most of the correlations developed in the literature are for annular flow situations. Extrapolation of the correlation to other flow patterns may be uncertain. As suggested by Hosler (1968), knowing the flow pattern in two-phase flow is analogous to the differences of laminar or turbulent flow in single-phase flow. Accordingly, the heat transfer/friction characteristics should be directly related to the flow pattern. The purpose of this study is twofold: firstly, to present new heat transfer/friction data for a tube having smaller tube diameter; secondly, to investigate the two-phase flow patterns inside the small tube, and seek a suitable flow pattern map that can describe the present data.

2. Experimental apparatus

The schematic of the experimental apparatus is depicted in Fig. 1. The test rig consists of two test sections, namely the heat transfer measurement test section and the flow pattern observation test section. The material of the test tube is copper, and the effective length of the test tube is 1.3 m for heat transfer measurement test section and 0.7 m for flow pattern obser-

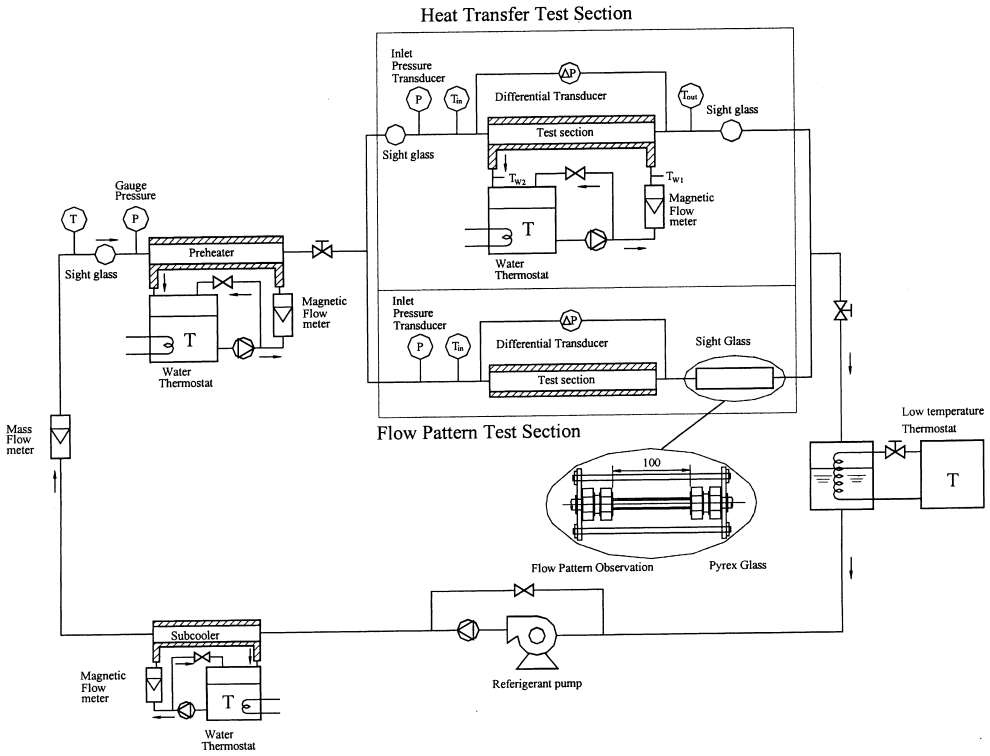

Fig. 1. Schematic diagram of test apparatus.

Table 1
Summary of estimated uncertainties

Primary measurements		Derived quantities		
Parameter	Uncertainty	Parameter	Uncertainty $G=100$ kg/m^2 s, $q=5$ kW/m^2	Uncertainty $G=400$ kg/m^2 s, $q=5$ kW/m^2
$\dot{m}_r$	0.3–1%	G	1.1%	0.5%
$\dot{m}_{water}$	0.5%	Re_i	0.6%	0.6%
ΔP	0.5%	ϕ_v^2	±8.3%	±2.6%
T	0.05°C	h	±9.4%	±12.4%

vation test section. The corresponding tube thickness of the test tube is 0.71 mm. Detailed descriptions of the test section can be found in the previous study of Kuo and Wang (1996) and Wang et al. (1997). Experiments were conducted using a commercially available 6.5 mm smooth tube. The heat transfer tests were conducted at two evaporation temperatures, namely 2°C and 7°C. In this study, R-22 is used as the working fluid, and its physical and transport properties are evaluated from computer program REFPROP (1996). Uncertainties of the heat transfer coefficients and friction factors reported in the present investigation, following the single-sample analysis proposed by Moffat (1988), are tabulated in Table 1.

3. Heat transfer data reduction

The heat duty for the test section was obtained from the flow rate and temperature drop of the water on the annulus according to the relation

$$\dot{Q} = \dot{m}_{water} Cp \Delta T. \tag{1}$$

The overall heat transfer coefficient was then computed from

$$U_o = \frac{\dot{Q}}{\mathrm{LMTD} \times A_o}, \tag{2}$$

where

$$\mathrm{LMTD} = \frac{\Delta T_1 - \Delta T_2}{\ln(\Delta T_1/\Delta T_2)}, \tag{3}$$

$$\Delta T_1 = T_{sat} - T_{water,out}, \tag{4}$$

$$\Delta T_2 = T_{sat} - T_{water,in}, \tag{5}$$

where T_{sat} is the saturation temperature of the refrigerant in the test section while $T_{water,in}$ and $T_{water,out}$ denote the inlet and outlet temperature of the water coolant on the annulus. The in-tube heat transfer coefficient was obtained from the thermal resistance equation

$$\frac{1}{U_o A_o} = \frac{1}{h_o A_o} + R_w + \frac{1}{h_i A_i}, \tag{6}$$

where h_o and h_i represent the average outside and inside heat transfer coefficients, and R_w denotes wall resistance. In the present calculation, the overall resistance is based on the outer surface area, which is evaluated as $\pi D_o L$, where D_o is the outside diameter of the test tube and L is the effective heat transfer length. The properties on the water side were calculated using average inlet and outlet bulk fluid temperatures. The determination of the inside heat transfer coefficient, h_i, requires knowledge of the outside heat transfer coefficient, h_o. This was accomplished by means of separate water-to-water tests on the same apparatus, with subsequent Wilson-plot analyses yielding the individual heat transfer coefficient relationships. The vapor quality entering the test section (x_{in}) is calculated from the energy balance on the preheater and the quality change in each test section is given by the energy balance

$$\Delta x = \frac{\dot{Q}}{\dot{m}_r \lambda} \tag{7}$$

and the average quality in each test section is given by

$$x_{ave} = x_{in} + \frac{\Delta x}{2}. \tag{8}$$

The heat transfer coefficient presented in this study is locally averaged value, and the increased quality in the test section is usually less than 0.13. The corresponding temperature rise on the water side ranged from 1.0°C to 3.3°C.

4. Flow visulation

As shown in Fig. 1, a sight glass is located at the end of the horizontal test section. The sight glass has a length of 100 mm having an internal diameter of 6.5 mm. Flow patterns are obtained from direct visual observations made from a microcamera.

Considerable differences exist in the definitions of two-phase flow patterns. Since the flow pattern identification by visual observation is subjective, it is essential that the flow patterns be defined in detail. Following the classification by Taitel (1990), the basic flow patterns inside a horizontal tube are divided into four main classes:

1. *Stratified flow:* The liquids flows at the bottom of the pipe with gas at the top. This flow pattern can be subdivided into stratified smooth (stratified) and stratified wavy (wavy) flow pattern.
2. *Intermittent flow:* The flow is in the form of liquid slugs which fill the pipe and are separated by gas zones in the form of elongated bubbles which contain a stratified liquid layer flowing along the bottom of the pipe. This flow pattern can be subdivided into plug and slug flow.
3. *Annular flow:* A liquid film flows adjacent to the pipe wall and the gas flows in the center core.
4. *Bubble flow:* Small discrete bubbles are distributed in a continuous liquid phase.

5. Pressure drop data reduction

The pressure drop data were analyzed using the concept of the two-phase multiplier. Tests were conducted adiabatically in the flow pattern observation test section. Because the acceleration pressure gradient, ΔP_a, can be neglected in the adiabatic experiments, a more accurate calculation of the frictional multiplier can be obtained. The multiplier is defined by:

$$\phi_v^2 = \frac{dP_f/dz}{dP_{f,G}/dz}, \tag{9}$$

where dP_f is the measured two-phase frictional pressure gradient and $dP_{f,v}$ is the frictional pressure gradients corresponding to the cases of vapor flowing alone in the channel. The multiplier was typically plotted versus vapor quality x or the Martinelli parameter X, where

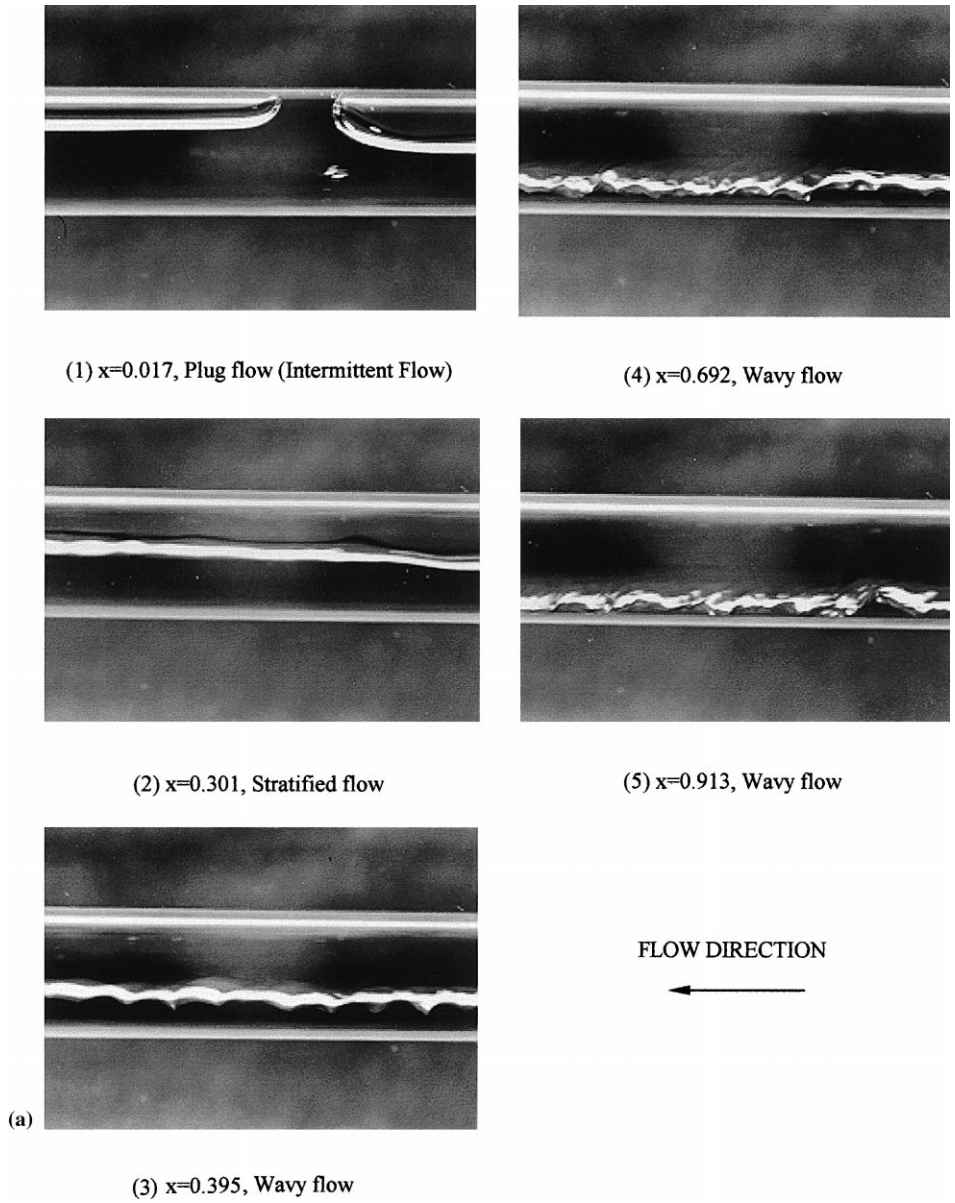

Fig. 2. Flow pattern for: (a) $G = 50$ kg/m^2 s; (b) $G = 200$ kg/m^2 s; (c) $G = 300$ kg/m^2 s; (d) $G = 700$ kg/m^2 s.

$$X = \sqrt{\frac{(\mathrm{d}P_{\mathrm{f,L}}/\mathrm{d}z)}{(\mathrm{d}p_{\mathrm{f,G}}/\mathrm{d}z)}}. \tag{10}$$

To verify the instrumentation and the measurement results, single-phase pressure drop data for R-22 give excellent agreement with the Blasius correlation for $\mathrm{Re_{Di}} > 8000$ ($0.079\ \mathrm{Re_{Di}^{-0.25}}$).

6. Results and discussion

Flow visualization tests were conducted for $G = 50$–700 kg/m^2 s. Photographs that are representative of the observed flow patterns and that correspond to mass flow velocities of 50, 200, 300, and 700 kg/m^2 s are given in Fig. 2(a)–(d), respectively, to show the progression from one flow pattern to the next. The main liquid–vapor interface is the white line. The flow patterns for $G = 50$ kg/m^2 s includes the plug, slug, and stratified flow pattern (stratified smooth and stratified wavy). Note that in this study the annular flow pattern is not seen for a mass velocity less than 100 kg/m^2 s. Further increasing of mass velocities to $G = 200$ kg/m^2 s results in plug/slug, stratified, wavy, and annular. Meanwhile, the liquid entrainment is clearly seen for the wavy and annular flow pattern for $G \geqslant 200$ kg/m^2 s which were not seen for the wavy flow pattern for $G = 50$ and 100 kg/m^2 s. The liquid entrainment becomes smaller as vapor quality further increases. For a mass flux of 300 kg/m^2 s, it can be observed that the plug/slug/wavy flow patterns are accompanied by the small vapor bubbles, and the bubble density increases with further increasing of mass flux. The flow patterns for $G = 700$ kg/m^2 s include the slug, wavy/annular, and annular flow pattern. As seen, the annular flow pattern becomes the dominant flow pattern as mass flux increases.

The observed flow patterns have been compared with several popular flow pattern maps, namely Baker (1954), Mandhane et al. (1974), and the VDI Heat Atlas (1993). The VDI flow pattern map is a modified flow pattern map of the well known semi-empirical flow pattern map proposed by Taitel and Dukler (1976). In summary, the Baker map gives the highest pre-

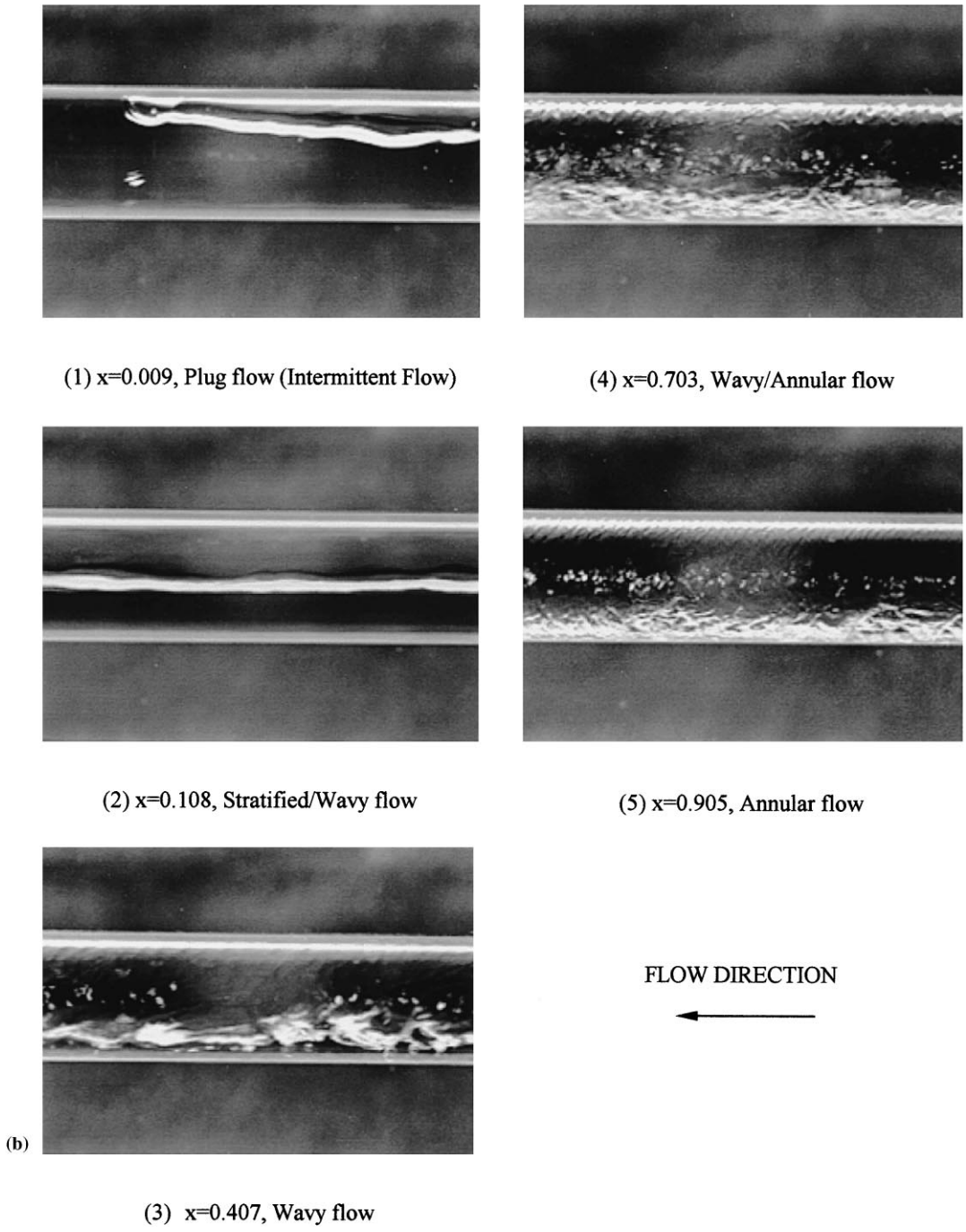

Fig. 2 (*continued*)

dictability (64%), the VDI map shows only 42% while the Mandhane one shows the poorest predictions (13%). The deviations between the above-mentioned flow pattern maps and the present data increase with the decrease of mass velocities. In the present study, we found that the line of transition to annular flow had shifted to lower gas superficial velocity. Lin and Hanratty (1987) reported a decrease of tube diameter will cause transition to annular at lower gas velocity.

Weisman et al. (1979) present extensive new data on the transitions between two-phase flow patterns during co-current gas liquid flow in horizontal lines. Systematic studies on the effects of liquid viscosity, liquid density, surface tension, gas density, and tube diameter were reported in this study. They proposed revised dimensionless correlations which fit their own data and previously available data with success. Their correlations can be summarized as follows:

Stratified-intermittent transition:

$$\frac{u_{GS}}{\sqrt{gD}} = 0.25\left(\frac{u_{GS}}{u_{LS}}\right)^{1.1}. \tag{11}$$

Stratified-wavy transition:

$$\left[\frac{\sigma}{gD(\rho_L-\rho_G)}\right]^{0.2}\left[\frac{Du_{GS}\rho_G}{\mu_G}\right]^{0.45} = 8\left[\frac{u_{GS}}{u_{LS}}\right]^{0.16}. \tag{12}$$

Transition to annular flow pattern:

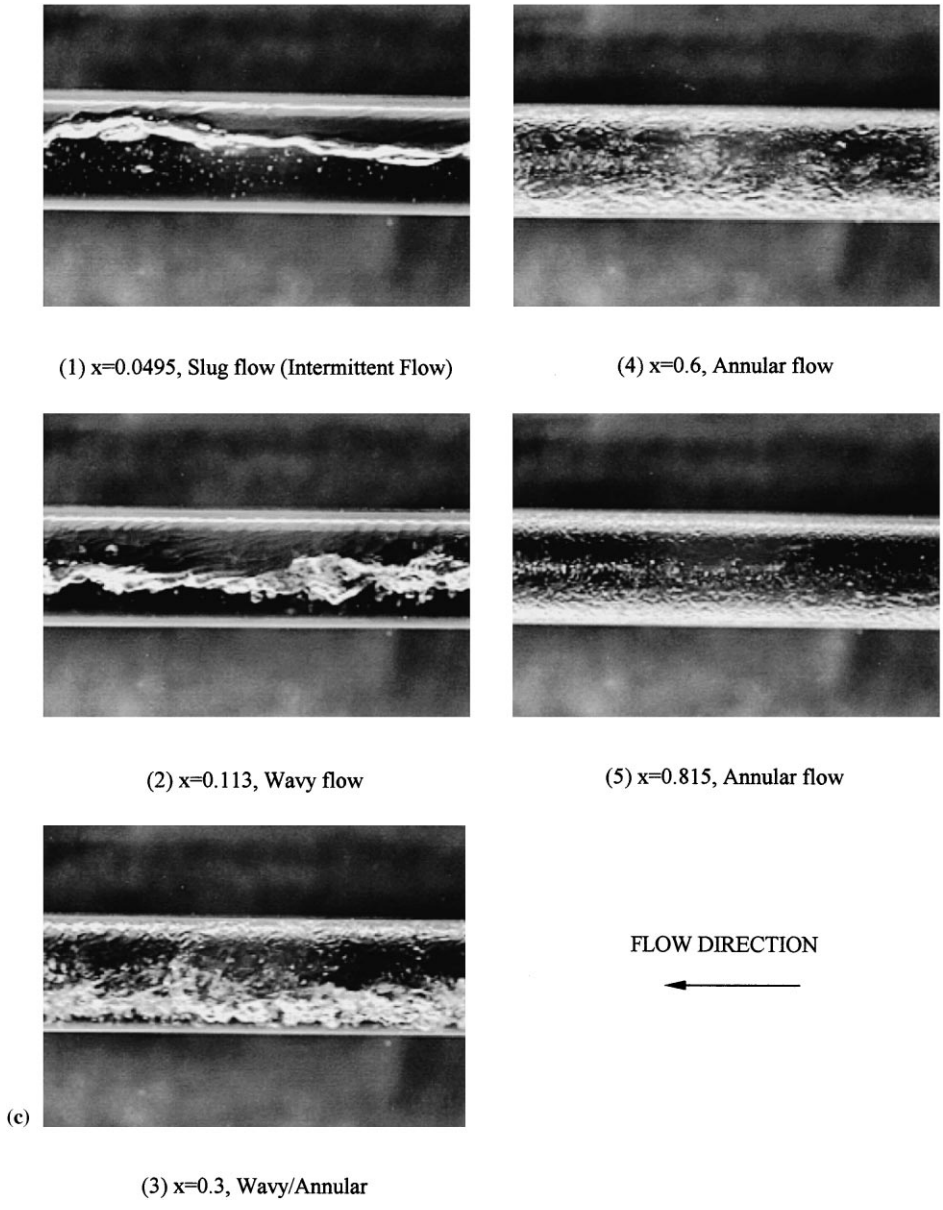

Fig. 2 (*continued*)

$$1.9\left[\frac{u_{GS}}{u_{LS}}\right]^{\frac{1}{8}}=\left[\frac{u_{GS}\rho_G^{0.5}}{[gD(\rho_L-\rho_G)\sigma]^{1/4}}\right]^{0.2}\left[\frac{u_{GS}^2}{gD}\right]^{0.18}. \tag{13}$$

Transition to dispersed flow pattern:

$$\left[\frac{(dP/dx)_L}{g(\rho_L-\rho_G)}\right]^{0.5}\left[\frac{\sigma}{g^2D(\rho_L-\rho_G)}\right]^{-0.25}=9.7. \tag{14}$$

Fig. 3 shows the present data with the Weisman et al. (1979) flow pattern map. It is shown that this flow pattern map gives very good agreements with the present test results, especially for the annular and intermittent flow pattern. Actually, 86% of the experimental data can be predicted by this map.

Klimenko and Fyodorov (1990) developed a mechanistic criterion for determining the transition from stratified to unstratified flow. They defined unstratified flow as all flow regimes with continuous wetting of the entire tube circumference. In this study, unstratified flow is annular flow. Based on a two-phase data bank, Klimenko and Fyodorov (1990) arrived at the following semi-empirical expression:

$$F=0.074\left(\frac{D_i}{b}\right)^{0.67}Fr_G+8\left[1-\left(\frac{\rho_G}{\rho_L}\right)^{0.1}\right]^2Fr_L. \tag{15}$$

For $F>1$, unstratified flow exists, and for $F<1$, stratified flow exists. They defined the Froude number for liquid and vapor phase using the superficial velocity,

$$Fr_L=\frac{\rho_L u_{LS}^2}{[(\rho_L-\rho_G)gD_i]}, \tag{16}$$

$$Fr_G=\frac{\rho_G u_{GS}^2}{[(\rho_L-\rho_G)gD_i]}, \tag{17}$$

and b is given as

$$b=\left[\frac{\sigma_L}{g(\rho_L-\rho_G)}\right]^{0.5}. \tag{18}$$

The criterion was transformed by Klimenko and Fyodorov (1990) to become a modified liquid and vapor Froude number, which is given by

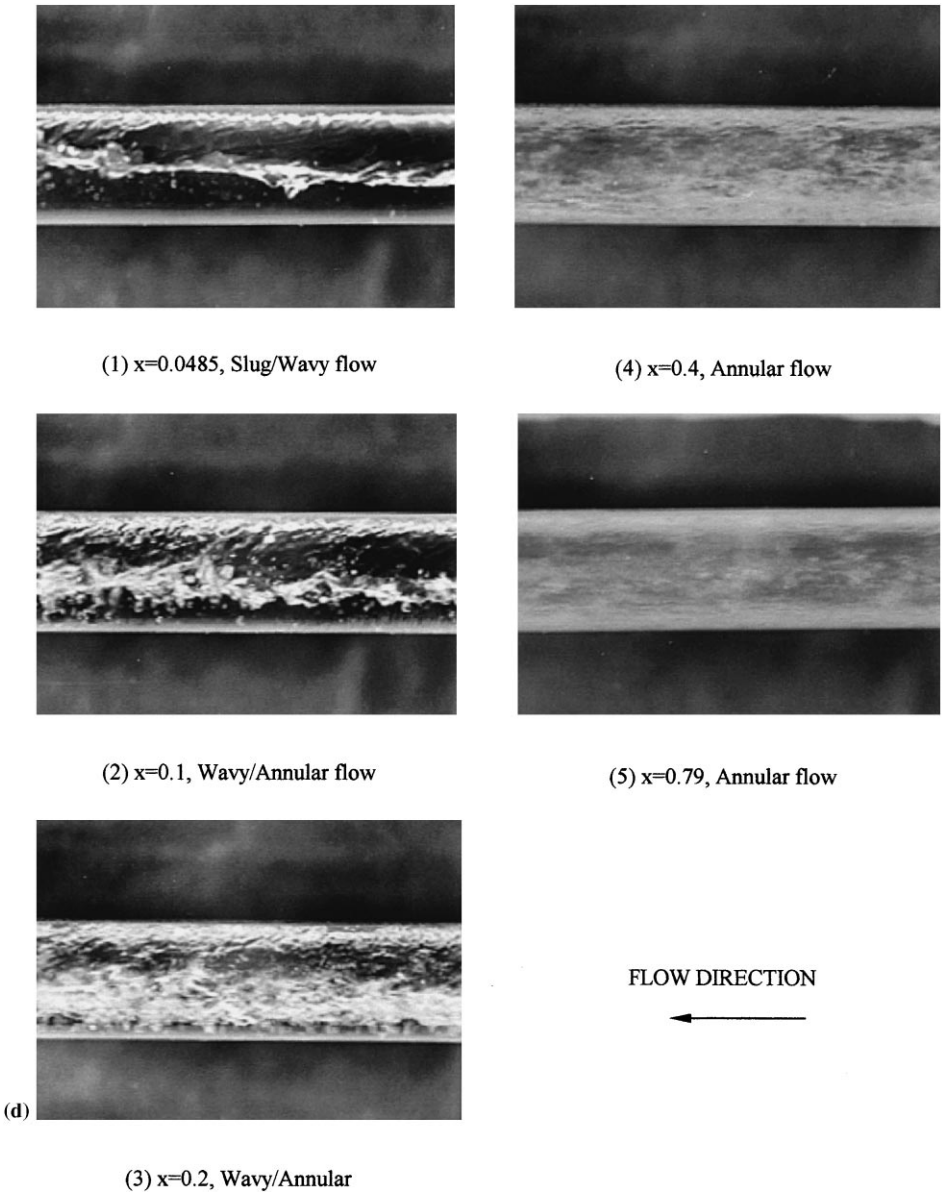

Fig. 2 (*continued*)

$$\mathrm{Fr}_{\mathrm{L,mod}} = \mathrm{Fr}_{\mathrm{L}}^{0.5}\left[1 - \left(\frac{\rho_{\mathrm{G}}}{\rho_{\mathrm{L}}}\right)^{0.1}\right], \tag{19}$$

$$\mathrm{Fr}_{\mathrm{G,mod}} = \mathrm{Fr}_{\mathrm{G}}^{0.5}\left(\frac{D_{\mathrm{i}}}{b}\right)^{0.33}. \tag{20}$$

Fig. 4 shows the present R-22 data plotted as modified Froude numbers. As seen from this figure, the simple criterion proposed by Klimenko and Fyodorov (1990) gives excellent classification of the present stratified and unstratified data.

For smooth, circular tubes, one may correlate the friction data using $\phi_{\mathrm{v}}^2 = \phi_{\mathrm{v}}^2(X)$. As proposed by Chisholm (1973),

$$\phi_{\mathrm{v}}^2 = 1 + CX + X^2, \tag{21}$$

where X is the Martinelli parameter, and is given by Eq. (10). For smooth tubes, the constant C ranges from 5 to 20, depending on whether the liquid and vapor phases are laminar or turbulent. In particular, the C factor can be adjusted to give a best fit to a given set of data. Fig. 5 shows the measured data plotted in the form ϕ_{v}^2 vs. X and values predicted by Eq. (21) for $C = 5$ and 20. Actually, C is strongly related to the observed flow pattern. A comparison between the observed flow pattern and the calculated two-phase multipliers shows that a constant of $C = 5$ may be more appropriate for the intermittent flow pattern. This is true even if the Reynolds number of both vapor and liquid phase are turbulent. For instance, for $G = 700$ kg/m^2 s, $x = 0.048$, the Reynolds numbers for liquid phase and vapor phase are 23990 and 17200, respectively, which are in the so-called turbulent–turbulent range. In the original Lockhard and Martinelli (1949) correlation, $C = 20$ is suggested. However, a considerable over-prediction is observed if $C = 20$ is used. In fact, a constant of 20 can describe the experimental data for $X < 0.2$ and $G \geqslant 200$ kg/m^2 s, which corresponds to the annular flow pattern. For a mass velocity greater than 200 kg/m^2 s, it is shown that the two-phase multipliers were insensitive to the change of mass velocity. However, for a mass velocity of 50 and 100 kg/m^2 s, the experimental data show a pronounced effect of mass velocity. This may be explained from wavy flow pattern in Fig. 2(a).

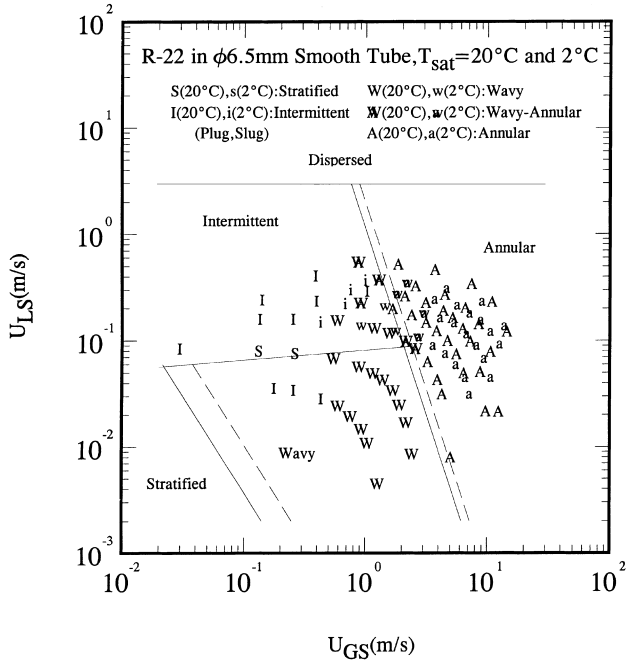

Fig. 3. Comparison with the present flow pattern with Weisman et al. (1979) flow pattern map.

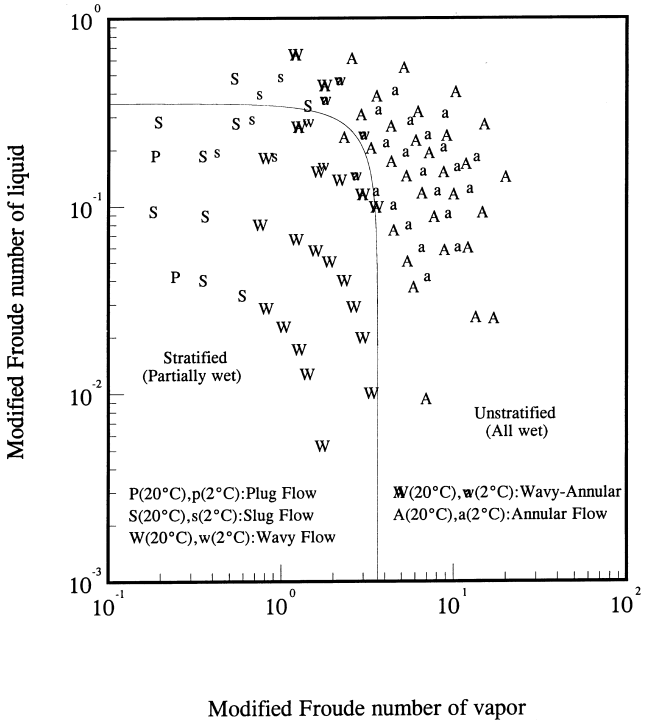

Fig. 4. Comparison with the present flow pattern data with Klimenko and Fyodorov (1990) criterion.

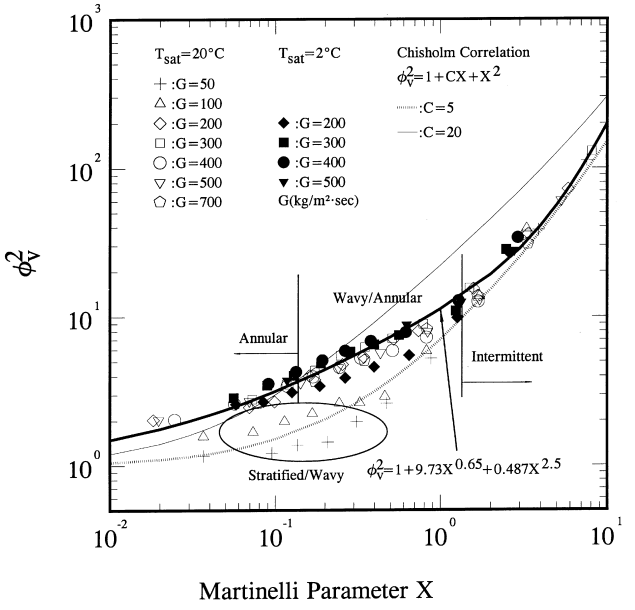

Fig. 5. Frictional multiplier vs. Martinelli parameter for the experimental data.

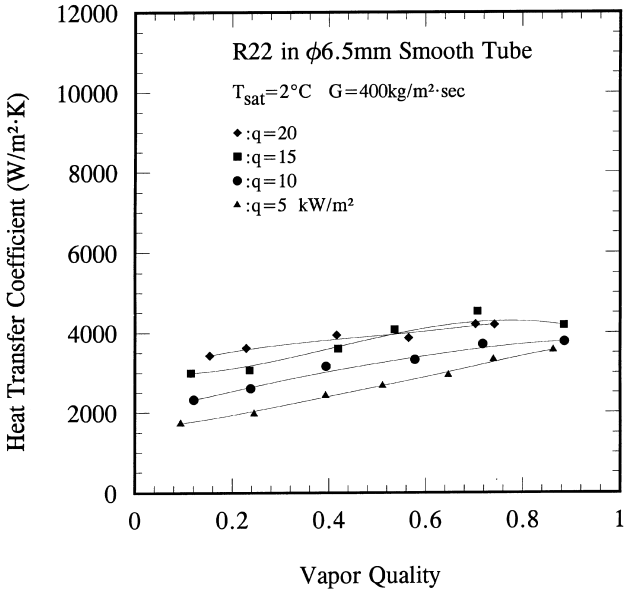

Fig. 6. Effect of heat flux on the evaporating heat transfer coefficient for $G = 400$ kg/m^2 s.

For $G = 50$ and 100 kg/m^2 s, the shear force at the vapor–liquid interface is not large enough, therefore, the amplitudes of the wave cannot reach top of the tube. This implies a partially wet phenomenon. Therefore, the friction characteristics may depend on the wetted perimeter which is affected by the mass velocity. Hence, a mass flux dependence was obtained. For $G > 200$ kg/m^2 s, the amplitude of the observed wavy flow pattern becomes high enough to reach the top (see the liquid streaks at the upper side of the wavy flow pattern). As a result, although the main flow pattern is wavy flow, the two-phase flow characteristics can be considered as "fully wet". Then, the effect of mass flux on two-phase multipliers may diminish.

Using a multi-regression process, the multiplier for $G \geqslant 200$ kg/m^2 s are correlated as

$$\phi_v^2 = 1 + 9.73X^{0.65} + 0.487X^{2.5}. \quad (22)$$

Note that Eq. (22) can correlate 91% of the data having mass velocities higher than 200 kg/m^2 s within ±20%. Also shown in the figure are data at mass velocities of 50 and 100 kg/m^2 s, the

two-phase multipliers are quite different from the prediction by Eq. (22). The mass flux shows a considerable effect on the two-phase multiplier. Therefore, the test results suggest that the C factor is not a constant but a function of Martinelli parameter and mass flux. Wambsganss et al. (1992) and Kuo and Wang (1996) also indicated this phenomenon. They proposed a modification on the C factor in the Chisholm (1973) correlation and the modified expression of C is given by

$$C = C(X, \mathrm{Re}_{\mathrm{LO}}) = aX^{\mathrm{b}}. \tag{23}$$

Therefore, using a multi-regression process, C can be correlated as

$$C = 0.00016121X^{-0.31}\mathrm{Re}_{\mathrm{LO}}^{1.23}. \tag{24}$$

Eq. (24) can describe 90% of the present data within ±20%.

Fig. 6 shows the variation of heat transfer coefficient versus quality with a fixed mass flux and varying heat flux ($G=400$ kg/m^2 s, $T_{\mathrm{sat}}=2$°C, $q=5$, 10, 15, and 20 kW/m^2, respectively). As expected, the heat transfer coefficients increase with the quality. This may be explained from the visual observation of flow patterns, for $G=400$ kg/m^2 s, changes from intermittent flow ($x<0.1$) to stratified wavy ($x<0.23$), and then finally annular flow pattern ($x>0.6$). Therefore, as the heat flux increases, the heat transfer coefficient increases in the low quality region owing to the nucleate boiling contribution, and eventually merges at higher qualities due to the suppression of the nucleate boiling component by the thinning of the annular liquid film. The present test results were compared with the correlation of Kandlikar (1990). Comparing with the measured data, the original Kandlikar (1990) correlation gives 35–80% overprediction. It appears the fluid dependent parameter in the Kandlikar correlation was obtained from a limited data source. Based on the present data, the fluid dependent parameter is approximately 1.43.

For a lower mass flux, $G=100$ kg/m^2 s, the flow patterns are intermittent flow and stratified flow. The effect of heat flux on the heat transfer coefficient is shown in Fig. 7. As seen, the effect of heat flux is more pronounced as compared with the results for $G=400$/kg m^2 s. Also, the heat transfer coefficients do not increase with increase of vapor quality. This indicates that the thinning of wavy liquid film does not effectively increase the heat transfer coefficient as compared to the annular flow pattern. The results may imply the major heat transfer mechanism for the partially wet stratified-wavy flow pattern may be due to nucleate boiling. This is different from the wavy flow pattern for $G=400$ kg/m^2 s. As explained earlier, the amplitude of the wave may reach the top of the tube. Therefore, the liquid streaks on the upper side of the tube increase the contribution of convective evaporation. A close examination of the present experimental data indicates that the two-phase heat transfer coefficient is proportional to $q^{0.6\text{–}0.7}$. The experimental data of Wattelet et al. (1994) and Ha and Bergles (1994) for a stratified-wavy flow pattern ($G=50$ kg/m^2 s) also show a heat flux dependence of 0.6–0.7. It is noted that for incomplete wetting the perimeter-averaged heat transfer coefficient shows a flat trend characteristics vs. vapor quality, and this phenomenon may become more pronounced as heat flux increases. The reported phenomenon is similar to those reported by the VDI Heat Atlas (1993). The correlation by Kandlikar (1990) suggests a smaller contribution of the heat flux. However, unlike the increasing heat transfer characteristics vs. quality, the Kandlikar (1990) correlation shows a flat trend characteristics which is similar to the present data. Kandlikar (1991) described this phenomenon in detail.

Fig. 8 shows the effect of mass flux at a fixed heat flux on the tube performance. For a prescribed heat flux ($T_{\mathrm{sat}}=7$°C and $q=5$ kW/m), the heat transfer coefficients increase with mass flux. However, the effect of mass flux is somewhat smaller for G lower than 200 kg/m^2 s. Doubling the mass flux from $G=100$ to 200 kg/m^2 s, the heat transfer coefficients increase with only 10–15% depends on the quality. The closing of heat transfer coefficients at low quality ($x<0.25$) for $G=100$, 200, and 400 kg/m^2 s is due to intermittent flow as observed from the pictures. For the intermittent flow pattern, the major heat transfer mechanism may be nucleate boiling. Further increase of mass flux from 200 to 400 kg/m^2 s shows a profound effect of mass flux. The average increase of heat transfer coefficient is about 55%. This may be due to the contribution of convective evaporation. The experimental data of Ha and Bergles (1994) show a similar result.

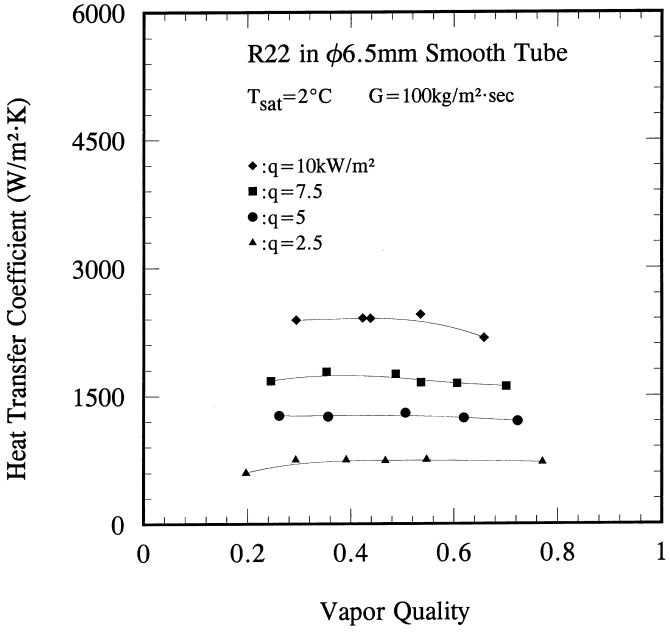

Fig. 7. Effect of heat flux on the evaporating heat transfer coefficient for $G=100$ kg/m^2 s.

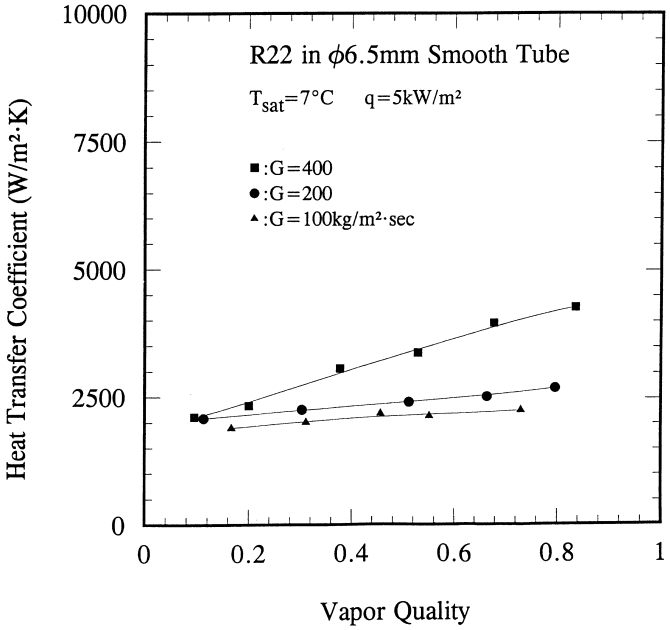

Fig. 8. Effect of mass flux on the evaporating heat transfer coefficient.

Fig. 9 shows the comparisons of the present average heat transfer coefficients with several other researches. The test results include those from Altman et al. (1960), Schlager et al. (1988), Sato et al. (1990), Kido et al. (1992), and Shin et al. (1997). Notice a considerable difference in the test conditions conducted by these investigators. For the present test data, the test conditions were $T_{sat} = 2°C$ and $q = 5$ and 10 kW/m. The present test results agree favorably with those by Kido et al. (1992) and Schlager et al. (1988). For $G < 200$ kg/m^2 s, the test results of Altman et al. (1960) are close to the present test results. For $G > 200$ kg/m^2 s, the test results by Altman et al. (1960) are significantly higher than the present data. It is interesting to note that their data showed a negligible effect of heat flux. It is not clear about this phenomenon. The test data by Shin et al. (1997) and Sato et al. (1990) are about 20–80% higher than the present test results. Possible explanations of this phenomenon may be due their higher saturation temperature and higher heat flux conditions. ($T_s = 12°C$ for Shin et al., 1997). The heat transfer coefficients for Sato et al. (1990) are considerably higher than the present results owing to their very smaller tube diameter ($D_i = 3.4$ mm) and very high heat flux.

7. Conclusions

Two-phase flow pattern, friction, and heat transfer characteristics for R-22 inside a 6.5 mm smooth tube are reported in this study. The range of mass flux is between 50 and 700 kg/m^2 s. Conclusions of the present study include:

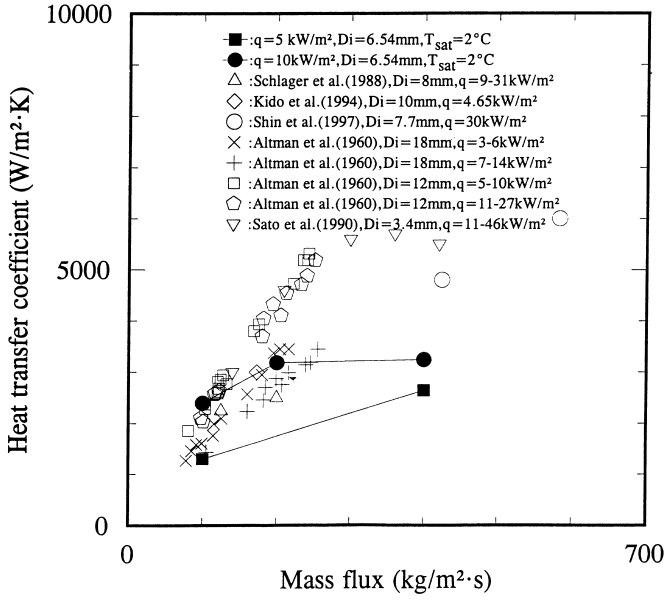

Fig. 9. Comparison of the present average heat transfer coefficients with other investigators.

1. In the range of this study, the flow pattern map proposed by Weisman et al. (1979) gave a satisfactory classification.
2. The simple criterion proposed by Klimenko and Fyodorov (1990) shows an excellent classification of the stratified and unstratified data.
3. The two-phase multipliers are strongly related to the flow pattern, and it is found that the two-phase multiplier is dependent upon mass velocities for the partially-wet stratified-wavy flow pattern. For intermittent, annular/wavy, and annular flow pattern, the two-phase multipliers is insensitive to mass flux.
4. The heat transfer coefficients for annular flow pattern increase with the increase of quality, and the effect of heat flux on heat transfer coefficient is suppressed at higher quality region. The major heat transfer mechanism for the partially-wet stratified-wavy flow pattern is nucleate boiling.
5. The heat transfer coefficient for intermittent flow pattern is insensitive to the change of mass flux.

Acknowledgements

The authors would like to express gratitude for the Energy R&D foundation funding from the Energy Commission of the Ministry of Economic Affairs for supporting this research work. The authors wish to thank Prof. Ralph Webb for providing valuable suggestions.

References

Altman, M., Norris, R.H., Staub, F.W., 1960. Local and average heat transfer and pressure drop for refrigerants evaporating in horizontal tubes. J. Heat Transfer 82, 189–198.

Baker, O., 1954. Design of pipe lines for simultaneous flow of oil and gas. Oil and Gas J. 53, 185–195.

Chisholm, D., 1973. Pressure gradient due to friction during the flow of evaporating two-phase mixtures in smooth tube and channels. Int. J. Heat Mass Transfer 16, 347–348.

Ha, S., Bergles, A.E., 1994. Some aspects of experimental in-tube evaporation. In: Proceedings of the Tenth International Heat Transfer Conference, vol. 6, pp. 187–192.

Hosler, E.R., 1968. Flow patterns in high pressure two-phase (steam-water) flow with heat addition. AIChE Symp. Ser. 64, 54–66.

Kandlikar, S.G., 1990. A general correlation for saturated two-phase flow boiling heat transfer inside horizontal and vertical tubes. J. Heat Transfer 112, 219–228.

Kandlikar, S.G., 1991. Development of a flow boiling map for subcooled and saturated flow boiling of different fluids inside circular tubes. J. Heat Transfer 113, 190–200.

Kido, O., Yoneda, H., Kan, H., Uehara, H., Miyara, A., 1992. Evaporation heat transfer and pressure drop of HCFC22 inside a horizontal rectangular channel – First report: Smooth surface (in Japanese). Transactions of JAR 9 (1), 33–42.

Klimenko, V.V., Fyodorov, M., 1990. Prediction of heat transfer for two-phase forced flow in channels of different orientation. In: Proceedings of the Ninth International Heat Transfer Conference, vol. 6, pp. 65–70.

Kuo, C.S., Wang, C.C., 1996. In-tube evaporation of HCFC-22 in a 9.52 mm micro-fin/smooth tube. Int. J. Heat Mass Transfer 39 (12), 2559–2569.

Lin, P.Y., Hanratty, T.J., 1987. Effect of pipe diameter on flow patterns for air–water flow in horizontal pipes. Int. J. Multiphase Flow 13 (4), 549–563.

Lockhard, R.W., Martinelli, R.C., 1949. Proposed correlation of data for isothermal two-phase two-component flow in pipes. Chem. Eng. Prog. 45, 39–48.

Mandhane, J.M., Gregory, G.A., Aziz, K.A., 1974. A flow pattern map for gas–liquid flow in horizontal pipeline. Int. J. Multiphase Flow 1, 537–553.

Moffat, R.J., 1988. Describing the uncertainties in experimental results. Exp. Therm. Fluid Sci. 1, 3–17.

REFPROP, 1996. Thermodynamic properties of refrigerants and refrigerant mixtures, version 5.0, Gaithersburg, MD. National Institute of Standards and Technology.

Sato, Y., Nosetani, T., Metoki, H., Morita, H., Kito, Y., 1990. Heat transfer performance of inner grooved copper tubes (in Japanese). Sumitomo light metal technical review 33 (1), 9–17.

Schlager, L.M., Pate, M.B., Bergles, A.E., 1988. Evaporation and condensation of refrigerant–oil mixtures in a smooth tube and a micro-fin tube. ASHRAE Transactions 94 (1), 149–166.

Shin, J.Y., Kim, M.S., Ro, S.T., 1997. Experimental study on forced convective boiling heat transfer of pure refrigerants and refrigerant mixtures in a horizontal tub. Int. J. Refrig. 20 (4), 267–275.

Taitel, Y., Dukler, A.E., 1976. A model for prediction of flow regime transitions in horizontal and near horizontal gas–liquid flow. AIChE J. 22, 47–55.

Taitel, Y., 1990. Flow pattern transition in two-phase flow. Paper presented at Ninth International Heat Transfer Conference, Jerusalem, pp. 237–254.

VDI Heat Atlas, 1993. Heat transfer to boiling saturated liquids. In: VDI Heat Atlas (in English), ch. Hbb1 and Hbb17, VDI-Verlag, Dusseldorf.

Wambsganss, M.W., Jendrzejczyk, J.A., France, D.M., 1991. Two-phase flow pattern and transition in a small, horizontal rectangular channel. Int. J. Multiphase Flow 17 (3), 327–342.

Wambsganss, M.W., Jendrzejcyk, J.A., France, D.M., Obot, N.T., 1992. Friction pressure gradients in two-phase flow in a small horizontal rectangular channel. Exp. Therm. Fluid Sci. 5, 40–56.

Wang, C.C., Chiang, C.S., Lin, S.P., Lu, D.C., 1997. Two-phase heat transfer characteristics for R-22/R-407C in a 6.5-mm smooth tube. Int. J. Heat and Fluid Flow 18 (6), 550–558.

Wattelet, J.P., Chato, J.C., Souza, A.L., Christofferson, B.R., 1994. Evaporative characteristics of R-12, R-134a, and a mixture at low mass fluxes. ASHRAE Transactions 100, part 1, 603–615.

Weisman, J., Duncan, D., Gibson, J., Crawford, T., 1979. Effect of fluid properties and pipe diameter on two-phase flow pattern in horizontal lines. Int. J. Multiphase Flow 5, 437–462.